Quantification of 5-HT$_{1A}$ receptors in human brain using *p*-MPPF kinetic modelling and PET

Sandra M. Sanabria-Bohórquez[1, 3], Francoise Biver[2], Philippe Damhaut[2], David Wikler[2], Claude Veraart[1], Serge Goldman[2]

[1] Neural Rehabilitation Engineering Laboratory, Université Catholique de Louvain, Brussels, Belgium
[2] PET/Biomedical Cyclotron Unit, Université Libre de Bruxelles – Erasme Hospital, 808, route de Lennik. 1070 Brussels, Belgium
[3] *Present address:* Merck Research Laboratories, 770 Sumneytown Pike, P.O. Box 4 WP44C-2, West Point, PA 19486, USA, e-mail: sandra_sanabria@merck.com, Tel.: +1-215-6522959, Fax: +1-215-6523667

Received 15 July and in revised form 30 September 2001 / Published online: 22 November 2001

Abstract. Serotonin-1A (5-HT$_{1A}$) receptors are implicated in neurochemical mechanisms underlying anxiety and depression and their treatment. Animal studies have suggested that 4-(2′-methoxyphenyl)-1-[2′-[*N*-(2′′-pyridinyl)-*p*-[^{18}F]fluorobenzamido] ethyl] piperazine (*p*-MPPF) may be a suitable positron emission tomography (PET) tracer of 5-HT$_{1A}$ receptors. To test *p*-MPPF in humans, we performed 60-min dynamic PET scans in 13 healthy volunteers after single bolus injection. Metabolite quantification revealed a fast decrease in tracer plasma concentration, such that at 5 min post injection about 25% of the total radioactivity in plasma corresponded to *p*-MPPF. Radioactivity concentration was highest in hippocampus, intermediate in neocortex and lowest in basal ganglia and cerebellum. The interactions between *p*-MPPF and 5-HT$_{1A}$ receptors were described using linear compartmental models with plasma input and reference tissue approaches. The two quantification methods provided similar results which are in agreement with previous reports on 5-HT$_{1A}$ receptor brain distribution. In conclusion, our results show that *p*-MPPF is a suitable PET radioligand for 5-HT$_{1A}$ receptor human studies.

Keywords: 5-HT$_{1A}$ receptors – *p*-MPPF – Kinetic modelling – PET

Eur J Nucl Med (2002) 29:76–81
DOI 10.1007/s00259-001-0684-2

Serge Goldman (✉)
PET/Biomedical Cyclotron Unit, Université Libre de Bruxelles – Erasme Hospital, 808, route de Lennik. 1070 Brussels, Belgium
e-mail: sgoldman@ulb.ac.be
Tel.: +32-2-5554720, Fax: +32-2-5554701

Introduction

Serotonin (5-hydroxytryptamine, 5-HT) is a central neurotransmitter and neuromodulator involved in various psychiatric and neurological disorders. Among the at least 14 different subtypes of 5-HT receptor, the 5-HT$_{1A}$ receptor is especially interesting because of its involvement in the neurochemical mechanisms underlying anxiety and depression and their treatment [1, 2]. Recently, several animal experiments have evaluated the *para*-fluorobenzoyl analogue of WAY-100635, 4-(2′-methoxyphenyl)-1-[2′-[*N*-(2′′-pyridinyl)-*p*-[^{18}F]fluorobenzamido] ethyl] piperazine (*p*-MPPF) [3], as a potential radioligand for positron emission tomography (PET) studies of 5-HT$_{1A}$ receptors. In vitro studies in rats using quantitative autoradiography [4] and in vivo evaluations in monkeys [5] and cats [6, 7] have demonstrated that *p*-MPPF labelling in the brain is reversible and characterised by very low non-specific binding. In addition, both the in vitro and the in vivo biodistribution of *p*-MPPF labelling is in total agreement with the known distribution of 5-HT$_{1A}$ receptors. Thus very high *p*-MPPF binding has been found in the hippocampus, cingulate cortex, entorhinal cortex, dorsal raphe nucleus and interpeduncular nucleus, and very low binding in the cerebellum [4, 5, 6, 7]. In addition, the lower affinity of *p*-MPPF for 5-HT$_{1A}$ receptors (K_i =3.3 n*M*) as compared with WAY-100635 (K_i =0.8 n*M*) [3] could make this new ligand sensitive to changes in endogenous serotonin concentration [8]. Considering these promising results, the aim of this study was to test the suitability of *p*-MPPF as an in vivo tracer of the human brain 5-HT$_{1A}$ receptors and to develop a reliable method for its quantification. The interactions between *p*-MPPF and 5-HT$_{1A}$ receptors were described using linear compartment models with both plasma input function and reference tissue [9, 10] approaches for modelling of the kinetic PET data.

Materials and methods

Subjects. Thirteen healthy volunteers, eight men and five women, aged 22–48 years (mean age 29.0±7.4 years) participated in the study. During a semi-structured interview, these subjects did not report any personal or familial major psychiatric or neurological disorder. They had no history of cranial trauma or drug or alcohol abuse. They did not present sleep disorders, had a normal diet and were under no medication. The five women were using hormonal contraceptives. Informed consent was obtained before the patients underwent the PET study. These experiments were approved by the Medical Ethics Committee of the Free University of Brussels.

Radiosynthesis of p-MPPF. The nitro precursor 4-(2′-methoxyphenyl)-1-[2′-[*N*-(2′′-pyridinyl)-*p*-fluorobenzamido]-ethyl] piperazine was supplied by the Cyclotron Unit of the University of Liege (Belgium). Labelled *p*-MPPF was prepared by a slight modification of the method described by Le Bars et al. [6, 11]. Ten milligrams of the nitro precursor in 900 ml of DMSO was added to the dry fluorinating agent [K/222]+^{18}F. The labelling reaction proceeded in an infrared oven by heating the reaction vial at 140°C for 10 min. After dilution with 40 ml of HCl 0.5 *M*, the activity was trapped on a conditioned C18 Sep-Pak VAC cartridge (100 mg), washed with 10 ml of HCl 0.5 *N* and eluted with tetrahydrofuran/methanol (60/40). The solution was diluted with 1.5 ml of acetate buffer (pH=5) and injected on high-performance liquid chromatography (HPLC) [symmetry C18 column from Waters eluted with MeOH/THF/aqueous 5×10^{-2} *M* NaOAc/HOAc (pH=5)]. The collected fraction was diluted ten times with 0.9% NaCl and passed through a conditioned C18 Sep-Pak VAC cartridge (100 mg). The latter was washed with 2×10 ml of saline and the activity was eluted with 1 ml of ethanol. The cartridge was rinsed with 10 ml of 0.9% NaCl and both fractions were passed through a 0.22-µm sterile filter and collected in a sterile evacuated vial.

Data acquisition. The subject's head was positioned in the scanner field of view as to obtain slices parallel to the canthomeatal line. Before the emission scan, a 10-min transmission scan was performed in each subject using a source filled with a [^{18}F]fluoride solution to correct PET images for attenuation. The experimental protocol lasted 60 min and consisted in an intravenous bolus injection of 3.7 MBq/kg (0.1 mCi/kg) of *p*-MPPF. The specific activity at injection time ranged from 37 to 148 MBq/pmol. Blood samples were collected from a catheter inserted in a radial artery to determine the kinetics of total plasma radioactivity and to follow the appearance of *p*-MPPF metabolites. Blood samples were manually withdrawn every 15 s for the first 2 min, every 30 s for the next 3 min, every 90 s up to 10 min, every 5 min up to 20 min, every 10 min up to 40 min and thereafter every 20 min until the end of the experiment. Blood samples were centrifuged for 5 min and total radioactivity was measured in plasma. The plasma curves were corrected for decay and expressed in nCi/ml. Brain tracer activity was measured with an eight-ring PET camera (CTI-Siemens 933-08-12, Knoxville, Tenn.), giving 15 contiguous transaxial slices. Spatial resolution of images is about 5 mm (full-width at half-maximum) in the tomographic direction and 7 mm in the axial direction. A sequence of 31 frames was obtained after tracer injection (6×10 s, 3×20 s, 4×30 s, 5×60 s, 6×120 s, 3×180 s, 2×300 s and 2×600 s). Images were reconstructed with a Hanning filter (cut-off frequency=0.5 cycles/pixel). The PET camera and the well counter used for the blood sample counting were calibrated every day using a cylindrical phantom containing a known amount of germanium-68 from which samples were taken for the well counter calibration.

Study of metabolites. To measure the metabolite levels in plasma, eight heparinised arterial blood samples (2–3 ml) were taken at 2, 5, 10, 15, 20, 30, 40 and 60 min post injection and were kept at 0°C. The blood samples were centrifuged (6,000 rpm, 5 min) and 1 µl of plasma was deproteinised by addition of 1 ml of acetonitrile and centrifugation (6,000 rpm, 5 min). HPLC analysis was performed by injection of 100 ml of the deproteinised plasma on a Waters Symmetry C18 column (5 mm, 3.9×150 mm + C18 Symmetry precolumn) eluted with tetrahydrofuran/methanol/water (NaOAc 5×10^{-2} *M*, pH=5) 17/28/55 at a flow rate of 0.6 ml/min. The effluent was collected for 15 min in 30-s fractions and counted in a gamma counter (Cobra autosampler, Canberra) [12].

Image analysis. Polygonal regions of interest (ROIs) were drawn manually on the PET image as follows. First, a summed PET image was obtained from the 31 frames after the *p*-MPPF injection. Then, ROIs were delineated using the image analysis program Mediman [13] by taking into consideration the activity on the summed PET image. Based on the human brain stereotaxic atlas of Talairach and Tournoux [14], ROIs containing at least 40 pixels were defined in the frontal cortex (Brodmann's areas 10–46), the hippocampus and the cerebellar cortex in both brain hemispheres. Special attention was paid to avoiding the inclusion of high blood volume structures (such as the venous sinuses) detected on the first frames of the dynamic scan in the delineated ROIs. ROIs were automatically projected on each frame to obtain the corresponding time-activity curves (TACs).

Kinetic modelling. Interactions between *p*-MPPF and 5-HT$_{1A}$ receptors were described using linear models consisting of two or three compartments with both plasma input function and reference tissue [9, 10] approaches. The three-compartment (3-comp) model includes the plasma space and two extravascular compartments representing the free and non-specifically bound MPPF ligand in tissue, $C_f(t)$, and the ligand specifically bound to 5-HT$_{1A}$ receptors, $C_b(t)$ (Fig. 1, top). The intravascular compartment represents the unchanged *p*-MPPF concentration in plasma, $C_p(t)$. With this model configuration, information on synaptic receptor density is obtained from the ratio k_3/k_4 or binding potential, *BP*. The 3-comp model was further reduced by lumping together the two tissue compartments (Fig. 1, bottom). This two-compartment (2-comp) model is described by two parameters, K_1 and k_2' (Fig. 1, bottom). The information on receptor concentration is obtained from the apparent distribution volume of the 2-comp model, *DV′*, obtained from the ratio K_1/k_2'. *DV′* can be expressed in terms of *DV* and *BP* of the 3-comp model as $DV'=DV(1+BP)$, where $DV=K_1/k_2$.

When the plasma input function approach (PIF model) was used to analyse the data, it was assumed that *p*-MPPF metabolites did not cross the blood-brain barrier (BBB). The rapid *p*-MPPF clearance from plasma (Fig. 2) prevented correct estimation of the tracer fraction at several of the time points in some of our experiments. Therefore, the estimation of the parent tracer fraction in plasma included data obtained at the University of Liege in four subjects (not participating in our study) after *p*-MPPF bolus injection. The mean *p*-MPPF fraction obtained from all subjects was then fitted to a bi-exponential function and individual $C_p(t)$ concentrations were obtained by multiplying the total plasma curve by the bi-exponential *p*-MPPF fraction function. The vascular contribution to the measured TAC was set at 5% in all ROIs and for all subjects [15].

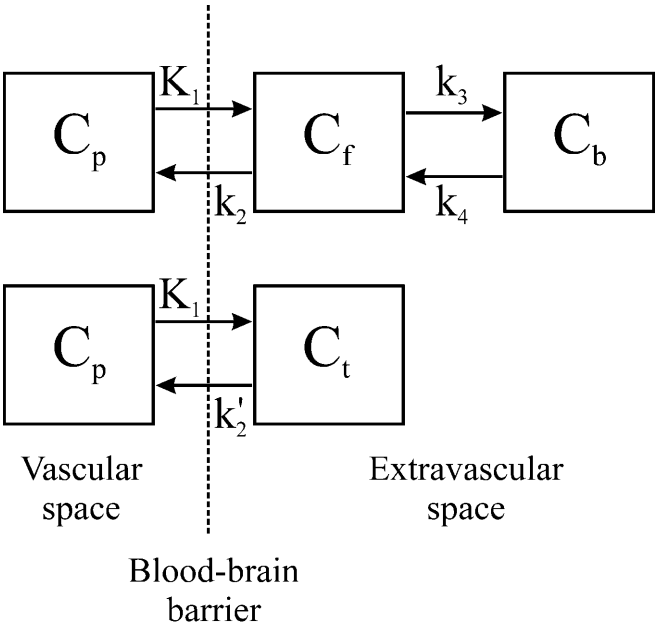

Fig. 1. Compartmental models for *p*-MPPF kinetics. The vascular compartment represents the concentration of unmetabolised ligand in plasma, C_p. The model at the *top* considers two extravascular compartments accounting for free ligand (and non-specifically bound ligand) in tissue, C_f, and *p*-MPPF specifically bound to 5-HT_{1A} receptors, C_b. In the two-compartment conformation (*bottom*), all tissular compartments are lumped together

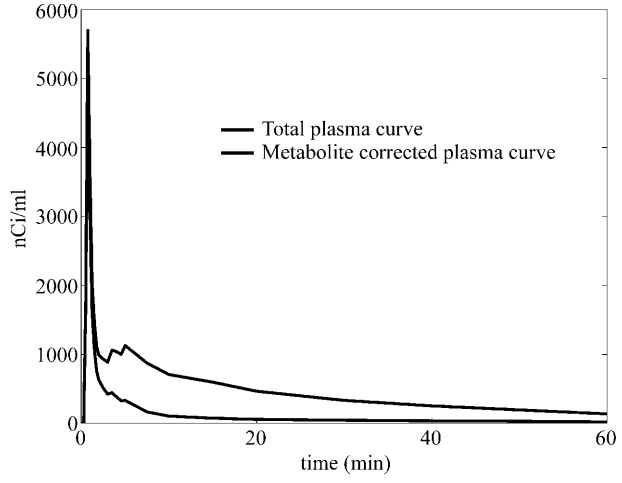

Fig. 2. Plasma TAC before and after correction for the appearance of metabolites, for a typical *p*-MPPF study. Rapid *p*-MPPF plasma metabolism meant that at 60 min following injection, only 17%±5% of the total radioactivity corresponded to unchanged tracer. Curves were corrected for isotope decay

The reference tissue approach constitutes a good alternative that allows avoidance of blood sampling during PET experiments by taking advantage of the very low *p*-MPPF binding observed in the cerebellum in in vitro and in vivo animal experiments [4, 5, 6, 7]. When data were analysed using this reference tissue approach, both 2-comp (simplified reference tissue model, SRTM) and 3-comp models (reference tissue model, RTM) were used to describe the target tissue region, and the 2-comp model to describe the reference cerebellar tissue region. RTM provides estimates for R_1, k_2, k_3 and *BP*, while SRTM does so for R_1, k_2 and *BP*. R_1 is the ratio of K_1 for target and reference regions. The vascular contribution to the TACs was neglected when applying RTM or SRTM methods.

Table 1. Model parameters

Model	Plasma input function	Reference tissue model
3-comp	K_1, k_2, k_3, k_4	R_1, k_2, k_3, *BP*
2-comp	K_1, DV'	R_1, k_2, *BP*

For the 3-comp models, the *BP* values were estimated from the ratio k_3/k_4

The set of compartmental parameters for each model configuration is detailed in Table 1. The cost function minimised to estimate model parameters was:

$$D(p) = \sum_{i=1}^{frames} w_i [Y(t_i) - y(t_i; p)]^2 \quad (1)$$

For each ROI, $y(t_i; p)$ corresponds to the modelled TAC. The experimental TAC, $Y(t_i)$, was obtained by Mediman and corresponds to the mean gamma activity concentration on the defined ROI corrected for ^{18}F decay. The weights w_i account for ROI mean statistics, frame length Δt_i [16, 17] and isotope decay:

$$w_i = \frac{\Delta t_i}{Y(t_i)} e^{-\ln(2) t_i / \tau} \quad (2)$$

where τ corresponds to ^{18}F half-life. Parameter coefficients of variation were obtained from the co-variance matrix resulting from the model sensitivity function matrix [17, 18]. The model equations were solved numerically by applying the Levenberg-Marquardt method [19] and implemented in MATLAB (The MathWorks, Inc., Natick, Mass.).

Results

The appearance of *p*-MPPF polar metabolites in plasma was relatively rapid. At 5 min, about 25% (n=7) of the total radioactivity in plasma corresponded to *p*-MPPF. This proportion reached about 15%±3% (n=7) at 10 min, 13%±4% at 30 min and 17%±5% at 60 min. Figure 2 shows the plasma TAC before and after correction for the appearance of metabolites, for a typical *p*-MPPF study.

Figure 3 shows two planes of a summed PET image after tracer injection in one of the subjects. The high *p*-MPPF labelling in the hippocampus allowed accurate localisation of this structure in the images. Intermediate labelling was observed in the neocortex and relatively low labelling in the cerebellum. The corresponding TACs in hippocampus, frontal cortex and cerebellum are shown in Fig. 4.

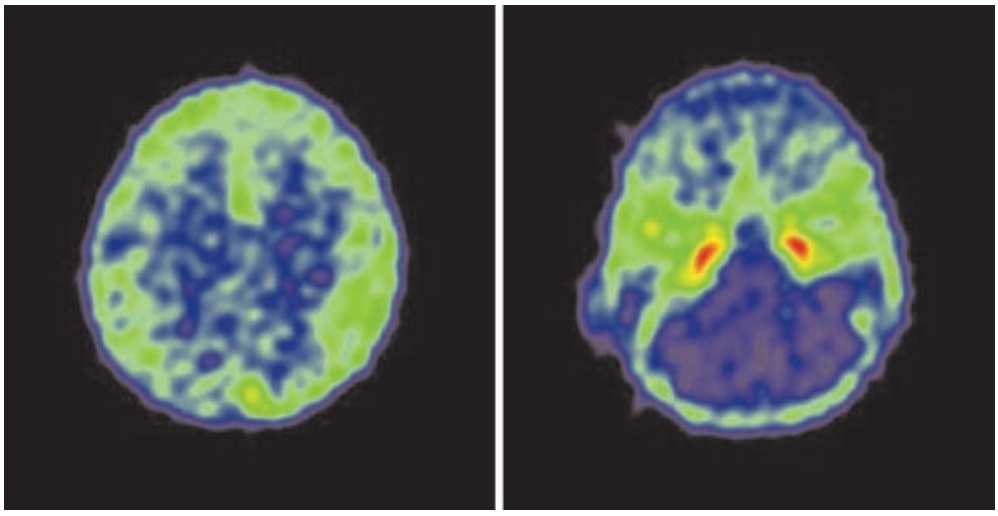

Fig. 3. Typical summed PET image from 13 to 40 min after bolus *p*-MPPF administration. Low binding was observed in cortical regions (*left*), whereas high accumulation was observed in the hippocampus (*right*). The lowest uptake was observed in the cerebellum (*right*)

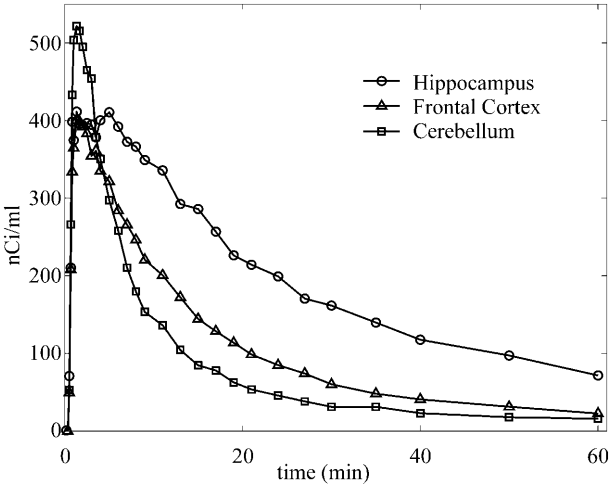

Fig. 4. Typical TACs of regional radioactivity after *p*-MPPF bolus injection for the hippocampus, frontal cortex and cerebellum. Curves were corrected for isotope decay

Table 2. Mean values ± SD for the 2-comp model parameters K_1 and *DV′* obtained when using the PIF model approach

ROI	*DV′*	K_1 (l/min)	*BP*
Hippocampus			
Right	1.216±0.185	0.082±0.021	1.594±0.274
Left	1.208±0.186	0.088±0.016	1.576±0.250
Frontal cortex			
Right	0.683±0.111	0.088±0.026	0.458±0.171
Left	0.676±0.107	0.090±0.023	0.442±0.159
Cerebellum			
Right	0.476±0.104	0.114±0.037	n/a
Left	0.459±0.078	0.121±0.045	n/a

BP values were estimated using the cerebellum as reference, $BP=DV'/DV_{ref}-1$. Vascular fraction was fixed at 5%
n/a, Not applicable

Kinetic modelling results

The parameter estimates obtained using the PIF approach with the 2-comp model are shown in Table 2. The highest *DV′* values were obtained for the ROIs in the hippocampus, followed by those in the frontal cortex and cerebellum. For all ROIs considered, K_1 and *DV′* were accurately estimated (unique solution and small parameter estimation uncertainties). SD values obtained from the co-variance matrix were below 10% for *DV′*, and mostly below 15% for K_1. The *BP* values for hippocampus and frontal cortex were determined using the cerebellum as the reference region, as $BP=DV'/DV_{ref}-1$. No difference was found between the *DV′* or *BP* values of female and male subjects (Fig. 5). When using PIF with a 3-comp model, it was not possible to find a unique solution for parameters K_1, k_2, k_3 and k_4 in any of the ROIs considered.

Tables 3 and 4 show the *BP* estimates using the RTM and SRTM approaches, respectively. *F* statistics analysis showed that the RTM had a significantly better fit ($P<0.05$) for 19 of the 52 ROIs considered (nine ROIs in the hippocampus and ten in the frontal cortex). However, a high inter-subject variability was observed for k_2 and k_3 when using the RTM. When using RTM or SRTM, the *BP* inter-subject variability was about 15% in the hippocampus and 35% in the frontal cortex, and, as with the PIF model, no difference was found between the *BP* values of female and male subjects in the examined regions (Fig. 5). A very good linear correlation was observed between the *BP* estimates with the two methods: $BP(RTM)=0.97BP(SRTM)+0.01$, $r^2=1.0$. As illustrated in Fig. 5, the *BP* estimates using RTM or SRTM were linearly correlated with the *BP* estimates obtained with the PIF model ($r^2=0.97$). However, *BP(RTM)* and *BP (SRTM)* appeared to be underestimated in comparison with the *BP* estimates using the PIF model.

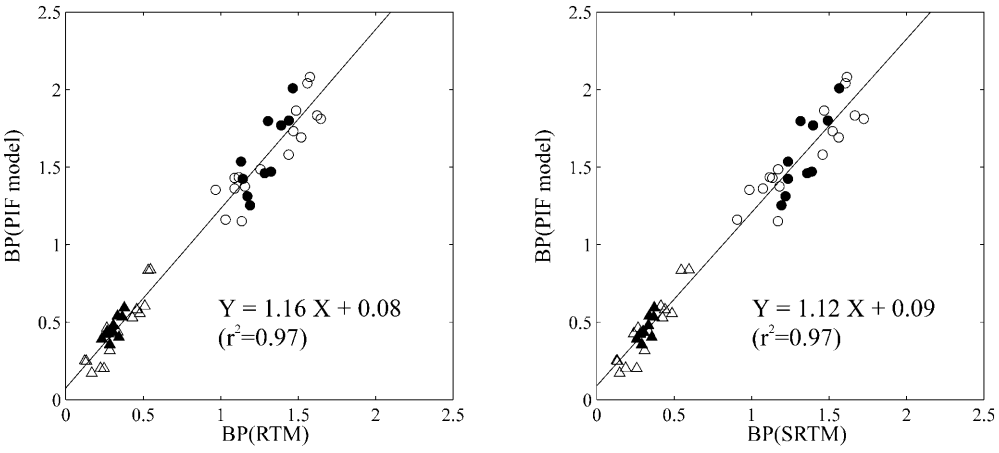

Fig. 5. Relation between *BP* values estimated using RTM or the PIF model (*left*) and SRTM or the PIF model (*right*) in the hippocampus (*circles*) and frontal cortex (*triangles*). *Filled symbols* correspond to the *BP* values in female subjects

Table 3. Mean values ± SD for the 3-comp model parameters when using the RTM approach

ROI	R_1	k_2 (l/min)	k_3 (l/min)	*BP*
Hippocampus				
Right	0.700±0.267	0.483±0.414	0.434±0.257	1.323±0.193
Left	0.818±0.149	0.288±0.135	0.443±0.156	1.301±0.190
Frontal cortex				
Right	0.702±0.157	0.414±0.384	0.185±0.078	0.334±0.117
Left	0.727±0.083	0.415±0.289	0.125±0.042	0.310±0.107

Table 4. Mean values ± SD for the 2-comp model parameters when using the SRTM approach

ROI	R_1	k_2 (l/min)	*BP*
Hippocampus			
Right	0.686±0.186	0.224±0.047	1.344±0.233
Left	0.722±0.140	0.226±0.060	1.330±0.196
Frontal cortex			
Right	0.648±0.139	0.303±0.092	0.333±0.119
Left	0.688±0.065	0.285±0.068	0.315±0.107

Discussion

We applied two kinetic approaches to quantify the binding potential of *p*-MPPF to 5-HT_{1A} receptors. The first approach, the PIF model, uses the concentration of ligand in plasma as a function of time, which is measured from continuous blood sampling during PET acquisition. Since *p*-MPPF metabolites are highly polar and since, as suggested by in vitro experiments, labelled metabolites crossing the BBB may not contribute significantly to the radioactivity measured in tissue [4], additional measurements are necessary to estimate the relative fraction of the parent in plasma. When applying the PIF model, it was not possible to identify two separate compartments (free and specific *p*-MPPF) from the tissue curves in any of the examined ROIs. Therefore, a one-tissue compartment providing robust *DV′* was used to quantify the *p*-MPPF binding. The mean and SD of *BP* calculated in the hippocampus using the PIF model and the cerebellum as the reference region were very similar to those recently reported in the literature using the linear graphical approach and the same reference region [20].

The second kinetic method presented here uses a reference tissue region devoid of receptors instead of plasma input function. Since low binding of *p*-MPPF has been observed in the cerebellum [4, 5, 6, 7], this region was used as a non-specific reference region when applying the RTM and SRTM approaches. Robust *BP* estimates (unique solution and low parameter uncertainties) were obtained when using RTM or SRTM. The SRTM adequately describes the *p*-MPPF kinetic data, and considering that the data analysis time is about one order of magnitude lower when using the reference region model with a 2-comp model rather than with a 3-comp model for the target tissue, the SRTM appears a very good alternative to RTM for modelling *p*-MPPF kinetics on an ROI or pixel-by-pixel basis.

Still, RTM- or SRTM-derived *BP* was underestimated as compared with the PIF model. Underestimation of *BP* by tissue reference region models has been recently modelled and discussed using simulations based on [^{11}C]WAY-100635 data [21, 22]. This underestimation may relate to violation of assumptions which underlie the RTM and SRTM methods. These assumptions essentially require that the reference region is devoid of specific binding and that, except for its binding on receptors, tracer behaviour is similar in all brain regions.

Apart from assumption violation, neglect of the vascular contribution to the reference region TAC is another possible cause of discrepancy between RTM or SRTM and PIF estimates of *BP*. The tight correlation between (S)RTM- and PIF-derived *BP* indicates that the reference region models offer a less invasive alternative to the PIF model, which requires arterial catheterisation. The regression slope of (S)RTM to PIF estimates is far closer to unity than those reported for [^{11}C]WAY-100635, and the *y* intercept is almost zero. This indicates that the reduced sensitivity of the RTM method for *BP* changes at high *BP* values is less critical for *p*-MPPF than for [^{11}C]WAY-100635, which is clearly advantageous for clinical applications. It should be kept in mind, however, that (S)RTM models may be intrinsically biased for pharmacological challenges that influence K_1, for instance if they induce differential blood flow changes in the target regions and the cerebellum. In such situations, PIF obviously remains the method of choice.

In conclusion, this study has shown the feasibility of using *p*-MPPF kinetic modelling to quantitatively assess the distribution of 5-HT$_{1A}$ receptors in the human brain using PET. Moreover, the low specific binding in the cerebellum permits the application of a simplified reference tissue approach to estimate the *p*-MPPF binding potential in different brain regions without blood sampling, which may be of great value in clinical studies of the serotoninergic function.

Acknowledgements. We wish to thank the staff of the PET/Biomedical Cyclotron Unit at the ULB for their assistance during data acquisition and processing. This work was supported by grants from the National Funds for Scientific Research (FNRS, Belgium) and the Medical Scientific Research Funds (FRSM, Belgium, grant 3.4547.96, 9.4509.96, 3.4533.94).

References

1. Peroutka SJ. Serotonin receptor subtypes. Their evolution and clinical relevance. *CNS Drugs* 1995; 4:18–28.
2. Saxena PR. Serotonin receptors: subtypes, functional response and therapeutic relevance. *Pharmacol Ther* 1995; 66:339–368.
3. Zhuang ZP, Kung M, and Kung HF. Synthesis and evaluation of 4-(2′-methoxyphenyl)-1-[2′-[*n*-(2″-pyridinyl))-*p*-iodobenzamido]-ethyl]piperazine *p*-MPPI: a new iodinated 5-HT$_{1A}$ receptor ligand. *J Med Chem* 1994; 37:1406–1407.
4. Plenevaux A, Weissmann D, Aerts J, Lemaire C, Brihaye C, Degueldre C, Le Bars D, Comar D, Pujo; JF, Luxen A. Tissue distribution, autoradiography, and metabolism of 4-(2′-methoxyphenyl)-1-[2′-[*n*-(2″-pyridinyl))-*p*-[^{18}F] fluorobenzamidoethyl] piperazine (*p*-MPPF), a new serotonin 5-HT$_{1A}$ antagonist for positron emission tomography: an in vivo study in rats. *J Neurochem* 2000; 75:803–811.
5. Shiue CY, Shiue GG, Mozley PD, Kung MP, Zhuang ZP, Kim HJ, Kung HF. *p*-MPPF: a potential radioligand for PET studies of 5-HT$_{1A}$ receptors in humans. *Synapse* 1997; 25:147–154.
6. Le Bars D, Lemaire C, Ginovart N, Plenevaux A, Aerts J, Brihaye C, Hassoun W, Leviel V, Mekhsian P, Weissmann D, Pujo JF, Luxen A, Comar D. High-yield radiosynthesis and preliminary in vivo evaluation of *p*-MPPF, a fluoro analog of WAY-100635. *Nucl Med Biol* 1998; 25:343–350.
7. Ginovart N, Hassoun W, Le Bars D, Weissmann D, Leviel V. In vivo characterization of *p*-MPPF, a fluoro analog of WAY-100635 for visualization of 5-HT$_{1A}$ receptors. *Synapse* 2000; 35:192–200.
8. Endres CJ, Carson RE. Assessment of dynamic neurotransmitter changes with bolus or infusion delivery of neuroreceptor ligands. *J Cereb Blood Flow Metab* 1998; 18:1196–1210.
9. Lammertsma AA, Hume SP. Simplified reference tissue model for PET receptor studies. *Neuroimage* 1996; 4:153–158.
10. Gunn RN, Lammertsma AA, Hume SP, Cunningham VJ. Parametric imaging of ligand-receptor binding in PET using the simplified reference region model. *Neuroimage* 1998; 6:279–287.
11. Plenevaux A, Lemaire C, Aerts J, Lacan G, Rubins D, Melega WP, Brihaye C, Degueldre C, Fuchs S, Salmon E, Maquet P, Laureys S, Damhaut P, Weissmann D, Le Bars D, Pujol J-F, Luxen A. [^{18}F]MPPF: a radiolabeled antagonist for the study of 5-HT1A receptors with PET. *Nucl Med Biol* 2000; 27:467–471.
12. Damhaut P, Plenevaux A, Lemaire C, Aerts J, Biver F, Monclus M, Luxen A, Goldman S. In vivo studies of *p*-[^{18}F]MPPF metabolites in human. *J Labelled Cpd Radiopharm* 1999; 42:S661–S662.
13. Coppens A, Sibomana M, Bol A, Michel C. MEDIMAN: an object oriented programming approach for medical image analysis. *IEEE Trans Nucl Sci* 1993; 40:950–955.
14. Talairach J, Tournoux P. *Co-planar stereotaxic atlas of the human brain*. New York: Thieme Medical, 1988.
15. Leenders KL, Perani D, Lammertsma AA, Heather JD, Buckingham P, Healy MJR, Gibbs JM, Wise RJS, Hatazawa J, Herold S, Beaney RP, Brooks DJ, Spinks T, Rhodes C, Frackowiak RSJ, Jones T. Cerebral blood flow and blood volume and oxygen utilization. Normal values and effect of age. *Brain* 1990; 113:27–47.
16. Delforge J, Syrota A, Mazoyer B. Experimental design optimization: theory and application to estimation receptor model parameters using dynamic positron emission tomography. *Phys Med Biol* 1989; 34: 419–435.
17. Delforge J, Syrota A, Mazoyer B. Identifiability analysis and parameter identification of in vivo ligand-receptor model from PET data. *IEEE Trans Biomed Eng* 1990; 37:653–661.
18. Cobelli C, DiStefano J. Parameter and structural identifiability concepts and ambiguities: a critical review and analysis. *Am J Physiol* 1980; 239:R7–R24.
19. Press WH, Teukolsky SA, Vetterling WT, Flannery BP. *Numerical recipes in C. The art of scientific computing*. New York: Cambridge University Press, 1994.
20. Passchier J, van Waarde A, Pieterman RM, Elsinga PH, Pruim J, Hendrikse HN, Willemsen ATM, Vaalburg W. Quantitative imaging of 5-HT$_{1A}$ receptor binding in healthy volunteers with [^{18}F]*p*-MPPF. *Nucl Med Biol* 2000; 27:473–476.
21. Stlifstein M, Parsey RV, Laruelle M. Derivation of [^{11}C]WAY-100635 binding parameters with reference tissue models: effect of violations of model assumptions. *Nucl Med Biol* 2000; 27:487–492.
22. Gunn RN, Lammertsma AA, Grasby PM. Quantitative analysis of [*carbonyl*-^{11}C] WAY-100635 PET studies. *Nucl Med Biol* 2000; 27:477–482.